CB
FDHMT

Optimization of electrically cooled complex HPGe Detector

Contract No. 4500109716

GSI Helmholzzentrum für Schwerionenforschung GmbH
Planckstraße 1
64291 Darmstadt

30. Mai 2012

CONTENTS

1. Introduction

The germanium crystals and the cold structure are installed in a vacuum cryostat where three processes, schematic presented in Fig. 1 determine the energy transfer between the room temperature cryostat walls and the low temperature assembly – heat radiation, thermal conductivity and residual molecular heating. A careful design of the components and appropriate material choice may substantially reduce the heat absorbed by the germanium crystals, thus making achievable the goals of electromechanically cooled HPGe (high purity germanium) detectors.

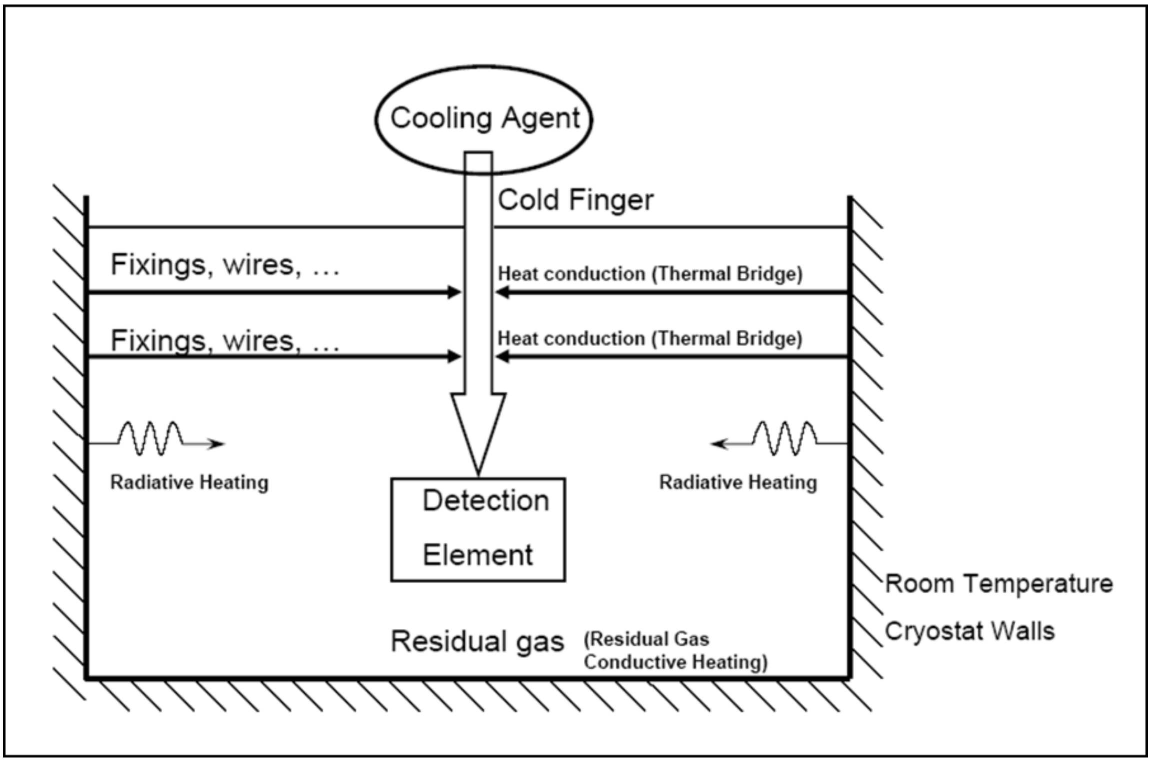

Fig. 1. Heat transfer schematic within the detector assembly.

The HPGe detectors are typically operated within the range of 77-110 K which determines a temperature difference between the warm cryostat walls and the cold frame of about 200 K. The assembly displayed on Fig.2 [1] possesses large surface of the detector cup surrounding the capsules hence predetermining an elevated radiative heating which may dominate even the overall heat transfer.

Beyond that, the warming impact of the thermal bridges, mechanical components used for fixing the cold structure to the warm section of the cryostat and the internal cabling between the crystal housing and the vacuum feedthrough may play substantial role. The fixing elements of the detector system under optimisation – labyrinths and spacers seem to be critical parts and an accurate dimensioning is needed in order to achieve minimal heat transfer at the same time preserving gamma-spectroscopy properties and the functionality required.

The space limitations impose minimal gap between the capsules assembly and the cryostat walls. However, at some critical gaps width, the residual gas of the evacuated inner space contributes significantly to the detectors warming and this effect depends on the vacuum level.

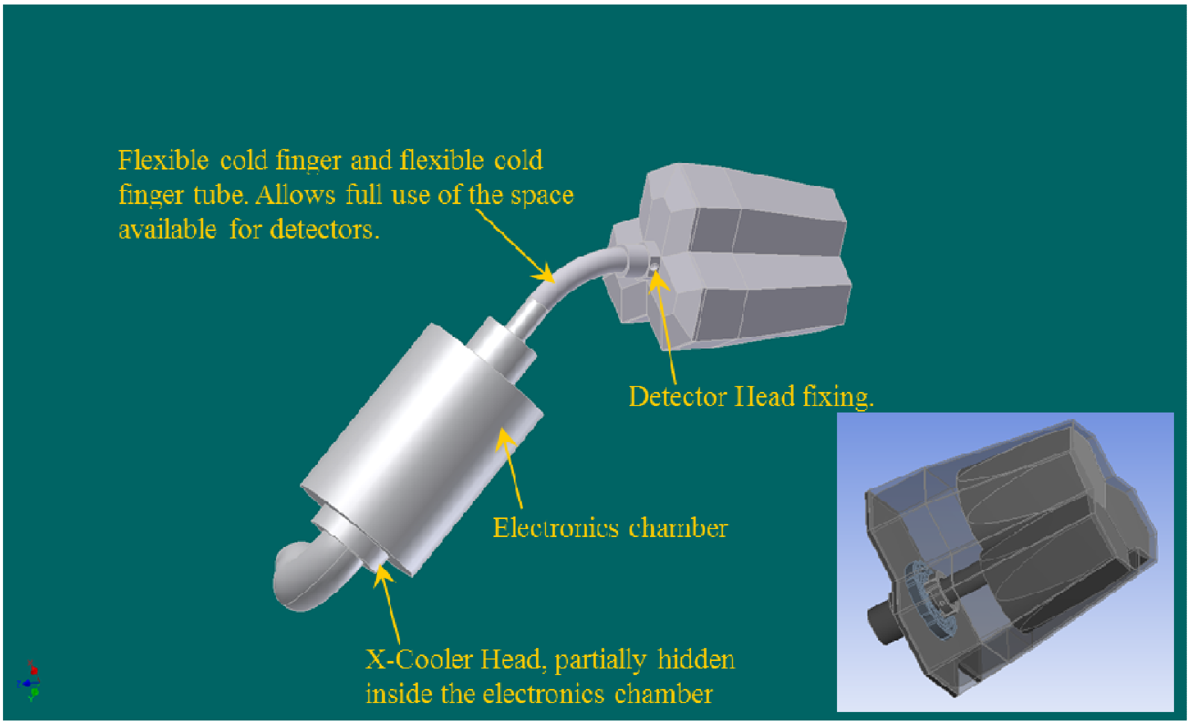

Fig. 2. Schematic drawing of the detector assembly.

It is worth to mention that some materials become brittle at cryogenic temperatures and thus the mechanical stability is no longer preserved. Other criterion observed by the material selection is the gases, water and hydrocarbons adsorption and the following releasing in vacuum. Appropriate metals are stainless steel, cooper, bras and aluminium. There are large number of plastics composites and ceramics suitable for operation in vacuum and at low temperature – e.g. PTFE, Mylar, Kapton, Vespel, Nylon, G10 (or FR4 – the glass-resin substrate for printed circuitry boards) and various resins.

The heat transfer within the interior domain of the assembly is being conducted under a broad temperature interval typically ranging from 77 K up to 300 K. The thermal conductivity displays a temperature dependent behaviour in such a wide-stretched domain and its values at room temperature may be not a good base for calculations.

In the assessment of the thermodynamic behaviour of the detector assembly the source data are of paramount importance. These data are often not well known (or even large discrepancies are observed between the authors) at cryogenic temperatures especially if a new material is applied. In this report the thermodynamic characteristics will be evaluated based on the data such as thermal conductivity, heat capacity, emissivity etc., collected and analysed by the NIST team. Some data from other sources also will be used when applicable.

The material selection is based on the components functionality and is specified to every particular component. For instance, to maximize the heat resistivity of the fixing labyrinth solid materials with extremely low thermal conductivity have been searched, that is critically discussed in paragraph **2.1**.

Heat capacity of the cold structure affects the detectors cooling respectively detectors warming dynamics. An important parameter is the holding time of the cold detector when the active cooling is switched off and how this time depends on the structure configuration. The time correlation for single, double, and etc. detectors assembly is reported in paragraph **2.2**.

Special attention to the thermal radiation at cryogenic temperature is drawn in paragraph **2.3**.

The enveloping surface area of the encapsulated Ge crystals toward the cryostat cup at triple and double detector configuration is relative large thus increasing the radiative heating which may exceed the cooling power of the engine. An intermediate thermal shield in the fashion it was made by the single capsule assembly is not a realistic solution because of the design complexity. As an alternative super insulation techniques is foreseen and discussed in paragraph **2.4**.

And at the end (paragraph **3**) the heat transfer within the HPGe Assembly accentuating on the material, shape and site optimisation of the fixing labyrinth is analysed.

2. Insulation materials under cryogenic temperature

2.1. Thermal conductivity

Minor differences of the material composition lead at cryogenic temperature to broadly divergent values of the thermal conductivity. The variations between the measured and the reported material properties are much greater than those at room temperature as well.

After critical analysis of the data available, a good approximation of the thermal conductivity *k*, suggested by NIST [3], is the following logarithmic equation,

$$log(\kappa) = a + b(logT) + c(logT)^2 + d(logT)^3 + e(logT)^4 + f(logT)^5 + g(logT)^6 + h(logT)^7 + i\,(logT)^8$$

Here T is the temperature, where a, b, c, d, e, f, g, h and I are the fitted coefficients, given in Table 1 for a few materials.

Coeff.	Teflon	Polyamide (Nylon)	Polyimide (Kapton)	G10 CR (norm)	G10 CR (warp)
a	2.7380	-2.6135	5.73101	-4.1236	-2.64827
b	-30.677	2.3239	-39.5199	13.788	8.80228
c	89.430	-4.7586	79.9313	-26.068	-24.8998
d	-136.99	7.1602	-83.8572	26.272	41.1625
e	124.69	-4.9155	50.9157	-14.663	-39.8754
f	-69.556	1.6324	-17.9835	4.4954	23.1778
g	23.320	-0.2507	3.42413	-0.6905	-7.95635
h	-4.3135	0.0131	-0.27133	0.0397	1.48806
i	0.33829	0	0	0	-0.11701
Data range	4-300 K	4-300 K	4-300 K	10-300 K	12-300 K

Table 1. Fitted coefficients for thermal conductivity for non-metals [3].

Kapton (Vespel), Teflon and Nylon are considered as potential candidates for the fixing labyrinth manufacturing. The thermal conductivity of the materials mentioned as a function of temperature is shown in Fig. 3.

As it is seen there the temperature dependent behavior of the conductivity is well pronounced. The thermal conductivity variations for Teflon are relatively small – from 0,24 [W/m.K] at 100 K up to 0,27 [W/m.K] at 300 K. This variation is stronger for Kapton where it increases from 0,14 [W/m.K] at 100 K up to 0,19 [W/m.K] at 300 K giving a relative rise of 35 %.

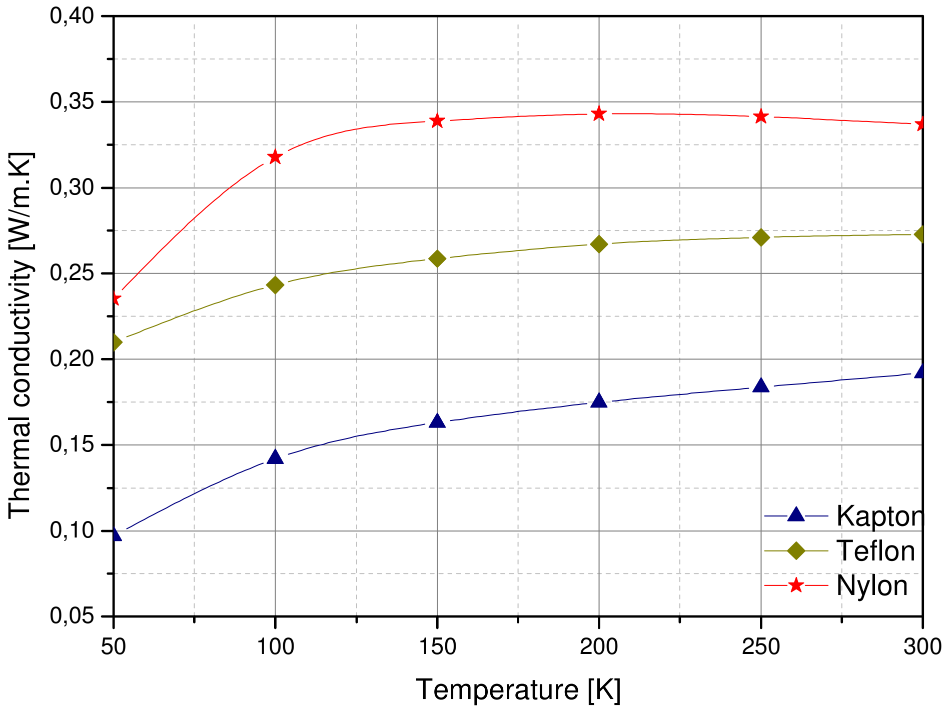

Fig. 3. Thermal conductivity as a function of temperature for some materials (Kapton, Teflon and Nylon).

Vespel, as a chemically close to Kapton plastic, also might be considered as a material suitable for the fixing labyrinth manufacturing, especially taking into account its gases and vapors adsorption/desorption properties at vacuum. The temperature dependent thermal conductivity data have been reported by Woodcraft and Gray [4] and hire are shown in Fig. 4.

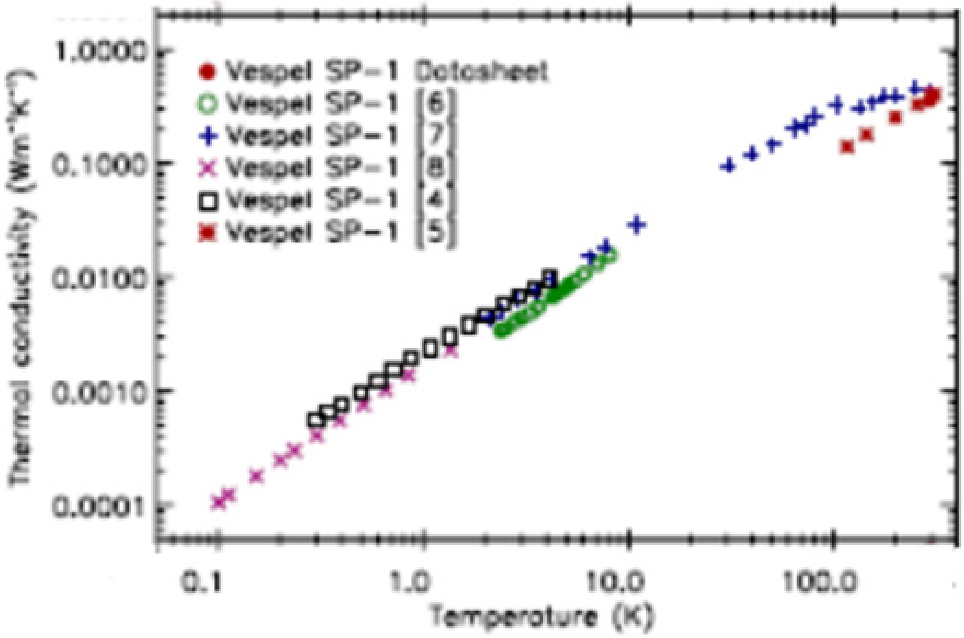

Fig. 4. Thermal conductivity of Vespel as a function of temperature [4].

The radiative energy transfer from the detector cup to the inner cold structure was identified as a dominant in the heat balance of the detector cryostat. Reduction of this transfer is made by thermal shield in the single detector assembly. The complexity of the overall detectors surface of the triple HPGe detector leads to enormous difficulties if a thermal shield is applied and even is feasible it may lead to high manufacturing cost. A possible solution can be thermally low conducting cup which may share substantially the thermal resistivity on the path “detector environment” – “cold structure”. A composite structure – for example resin-fiberglass composition or aluminum-fiberglass-resin composition may satisfy this requirement. Other materials must be sought in order to achieve reasonable results.

The cryostat cup of the single electromechanically cooled HPGe detector has been fabricated from aluminum alloy [5-7]. Thermodynamically aluminum and fiberglass-resin composition are differently classified. While aluminum is a good conducting material, fiberglass-resin composition possesses relative low thermal conductivity. The cup wall is a part of the heat transfer path and when made of highly conductive materials its thermal resistivity is usually neglected.

The evaluation of the thermal conductivity of the cryostat cup made of low thermal conductivity materials is done, based on G-10 fiberglass-resin composition and glass fabric polyester. The temperature dependent conductivity of G-10 fiberglass-resin composition has been calculated after Marquardt et al [3] and graphically given in Fig. 5. It is to mention that fiberglass-resin composition materials possess anisotropic thermodynamic behavior which is to be seen in the figure below.

Thermal conductivity of resin materials vary in dependence of their composition. In order to give some idea of how the thermal conductivity varies, two compositions are considered and their thermal conductivity as a function on temperature is graphically given in Fig. 6.

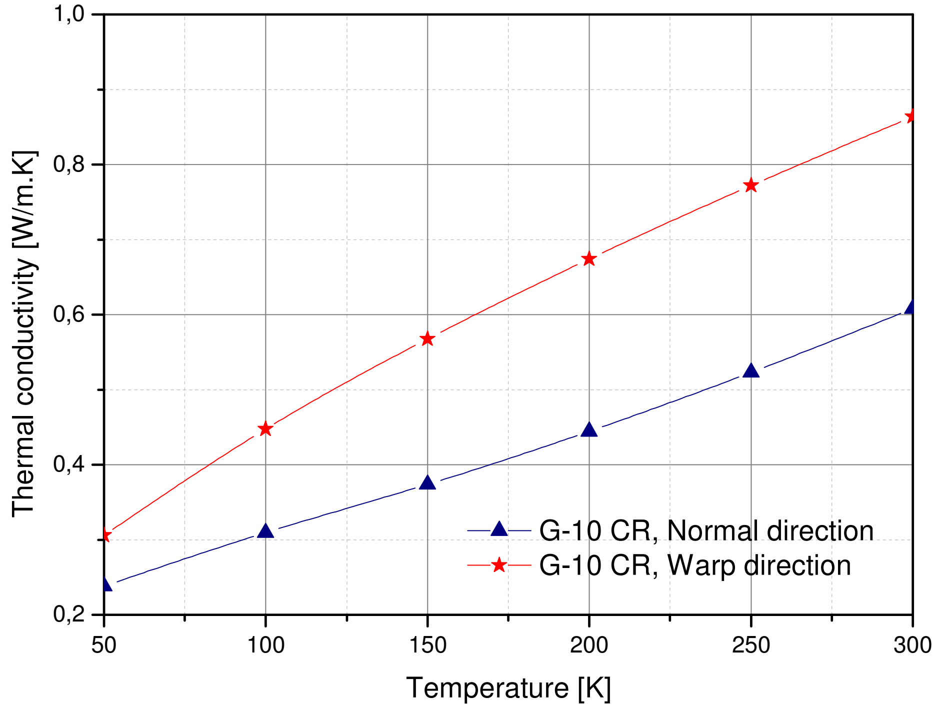

Fig. 5. Thermal conductivity as a function of temperature and direction for G-10 fiberglass epoxy.

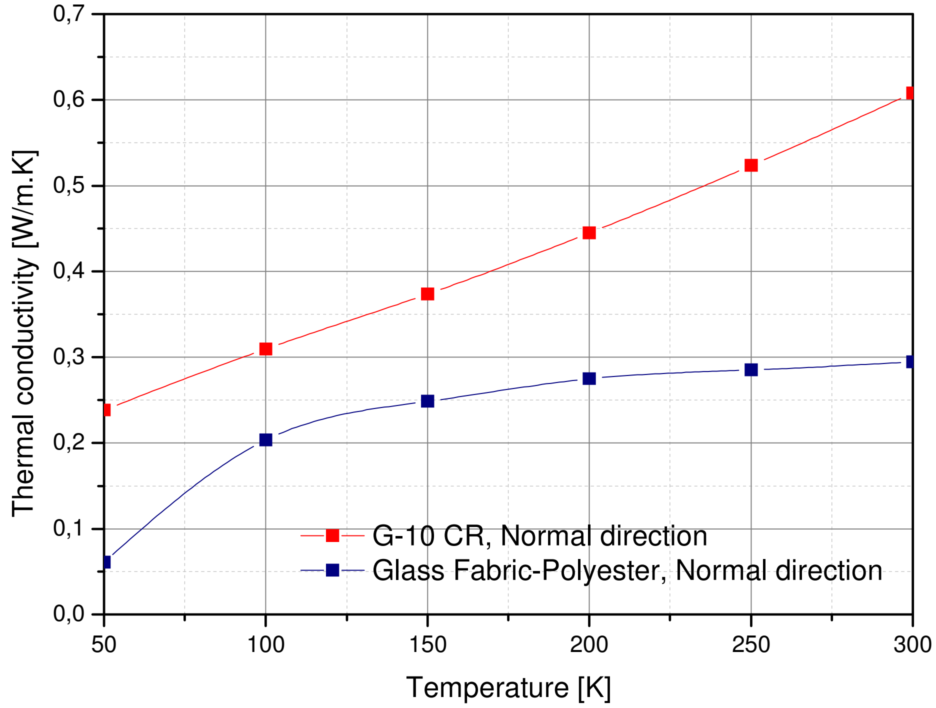

Fig. 6. Thermal conductivity for two different epoxy materials.

The analysis taking into account the thermal conductivity of the detector cup is based on the thermal flux balance and leads to the following expression for the temperature difference across the wall thickness and the flux:

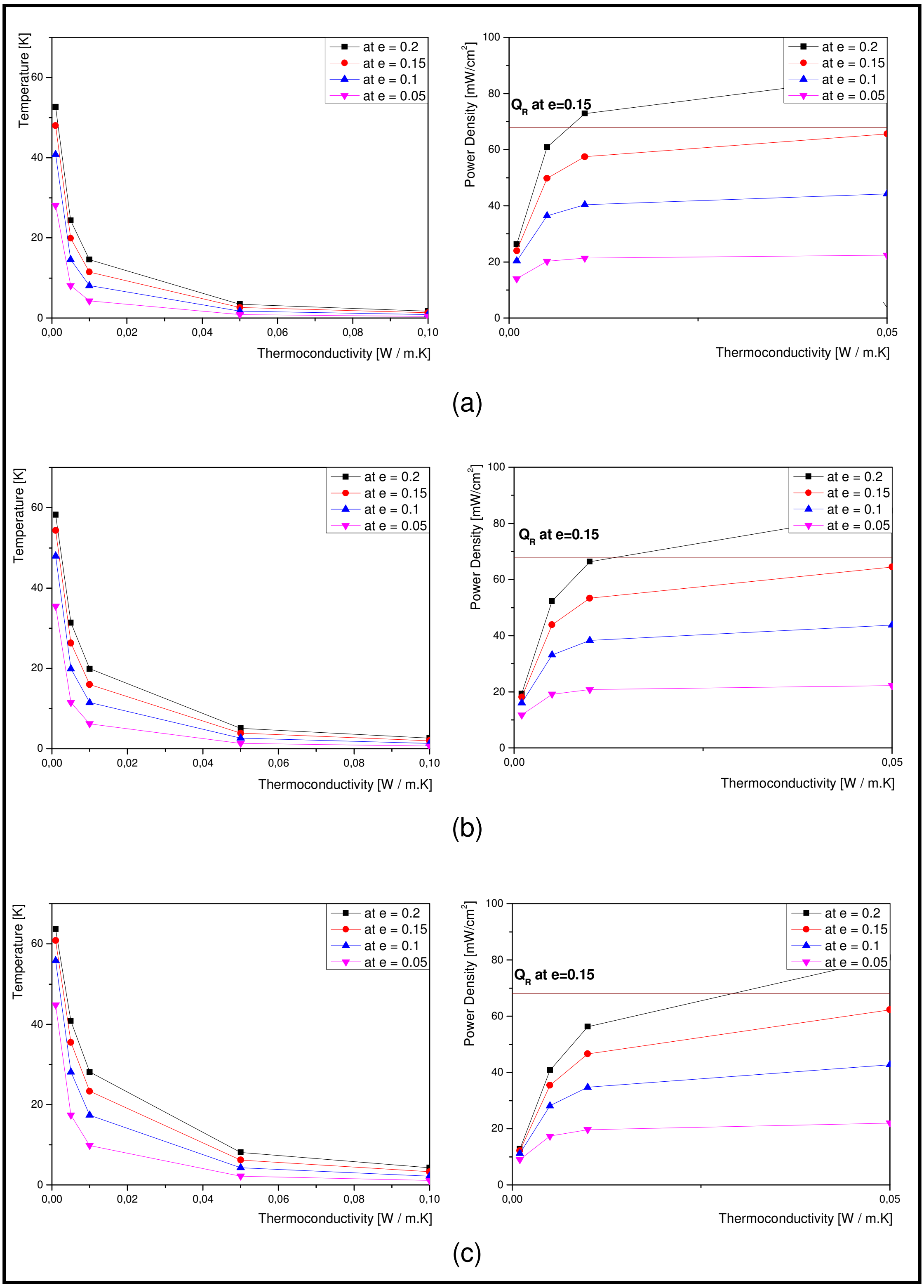

Fig.7. The temperature difference ΔT and the flux Q as a function of the emissivity ε, and the thermal conductivity k at detector cup thickness of 2 mm (a); 3mm (b) and 5 mm (c). The radiative transfer limits are given for ε=0.15.

$\Delta T = \frac{d}{A+1{,}35\cdot 10^{-2}d}$ $[K]$

$Q = \frac{k}{A+1{,}35\cdot 10^{-2}d}$ $[\frac{W}{m^2}]$

Where $A = \frac{k}{0{,}454\ \varepsilon}$ and d is the wall thickness (in mm), k is the thermal conductivity in W/m.K and ε is the emissivity of the cold structure. Below k=0.05 W/m.K the conductive component of the thermal resistivity is not negligible and can substantially reduce the whole thermal flux. The results for ΔT and Q are plotted on Fig. 7 for 2, 3 and 5 mm thickness of the detector cup wall.

Based on these results a conclusion can be made that the fiberglass materials does not possess such properties and therefore another material have to be sought. There are some plastics with k < 50 mW/(m.K), however, their radiation hardness has to be considered as well. Optionally, a “sandwich” construction (if it helps considerably to reduce the thermal burden) may be a suitable choice.

2.2. Heat capacity and thermal expansion

Heat capacity and thermal expansion are also important, though usually not as critical as thermal conductivity. In contrast of the conductivity they are not very sensitive to small variations in material compositions.

The heat capacity is a strong function of the specific heat which depends on the temperature. At room and lower temperatures this dependence is not essential; however, approaching cryogenic temperatures (below 100 K) the function becomes stronger as graphically shown in Fig. 7 (taken from [3]). In practice heat capacity presupposes the time needed thermodynamical equilibrium of the system to be reached.

The heat capacity affects not only the cooling time of the detector assembly, but also the “temperature timeout”, i.e. the time when the temperature does not rise much after the active cooling is switched off. This “temperature timeout” allows handling of the cold detector without “short cycling” (partial warming up of the detector) to happen, e.g. installation on the setup, transportation between the Lab and the experimental site etc.

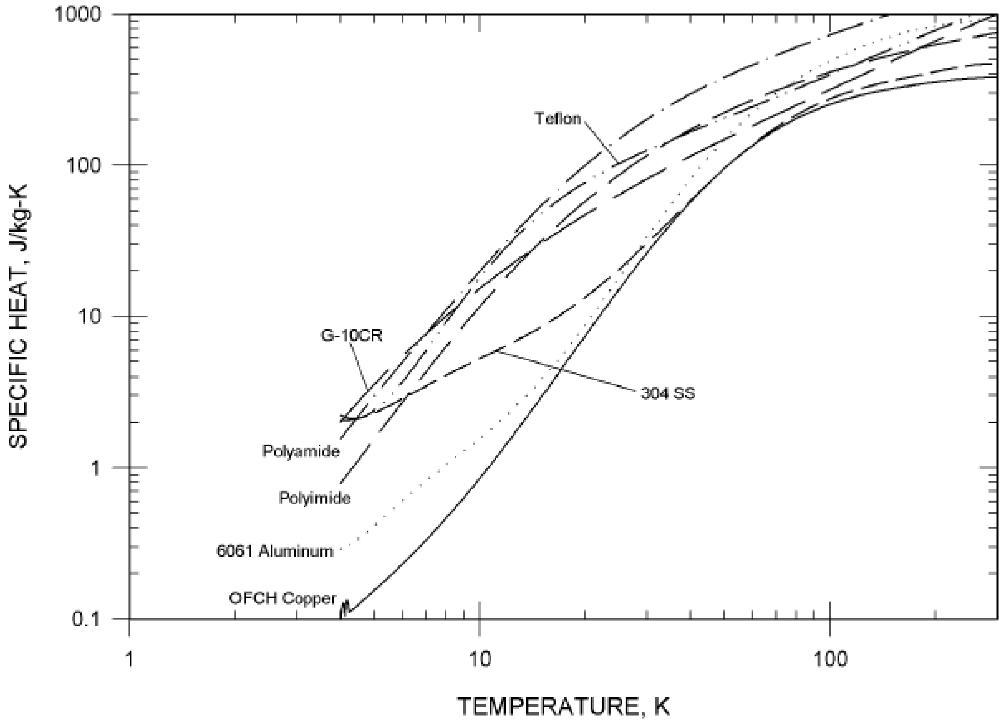

Fig. 7. Specific heat of various materials [3].

Estimation of the "temperature timeout" is based on the material properties of Germanium given in Table 2.

Density [kg/m³]	5330
Heat capacity [J/kg.K]	320

Table 2. Germanium material properties

It has been supposed that the temperature of the cold part is T_0 while the temperature of the warm part is T_∞. The overall detector surface (A) and the volume (V) are specified in Table 3 in dependence of the detectors type.

Detector type	**Overall surface** [m²]	**Volume** [m³]
Single	0.030484	0.00028
Double	0.055326	0.00056
Triple	0.074526	0.00084
Quartet	0.088084	0.00112

Table 3. Detectors geometric specification.

The warming uptime is described by the following formulae below

$$t_{warming} = t_{ref}\left[\frac{1}{4}\cdot ln\frac{(1+\theta)(1-\theta_0)}{(1-\theta)(1+\theta_0)} + \frac{1}{2}arctan\theta - \frac{1}{2}arctan\theta_0\right],$$

where the reference time is $t_{ref} = \frac{\rho c}{\varepsilon\sigma T_\infty^3}\cdot\frac{V}{A}$ and $\theta_0 = \frac{T_0}{T_\infty}$, $\tau = \frac{t}{t_{ref}}$ and the dimensionless temperature $\theta = \frac{T}{T_\infty} = \frac{T_0+\Delta T}{T_\infty}$.

Some typical cases are shown in the Fig. 8-9. Here the temperature of the cold part is considered to be 77 K, while the temperature of the warm part 300 K.

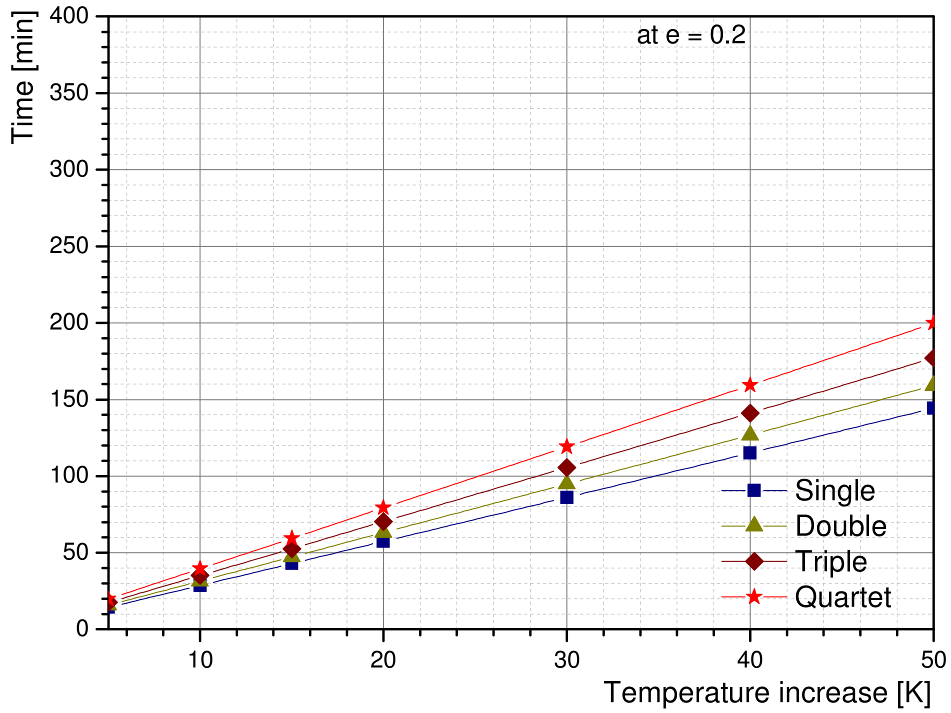

Fig. 8. Temperature development in dependence on detector configuration and ε=0.2.

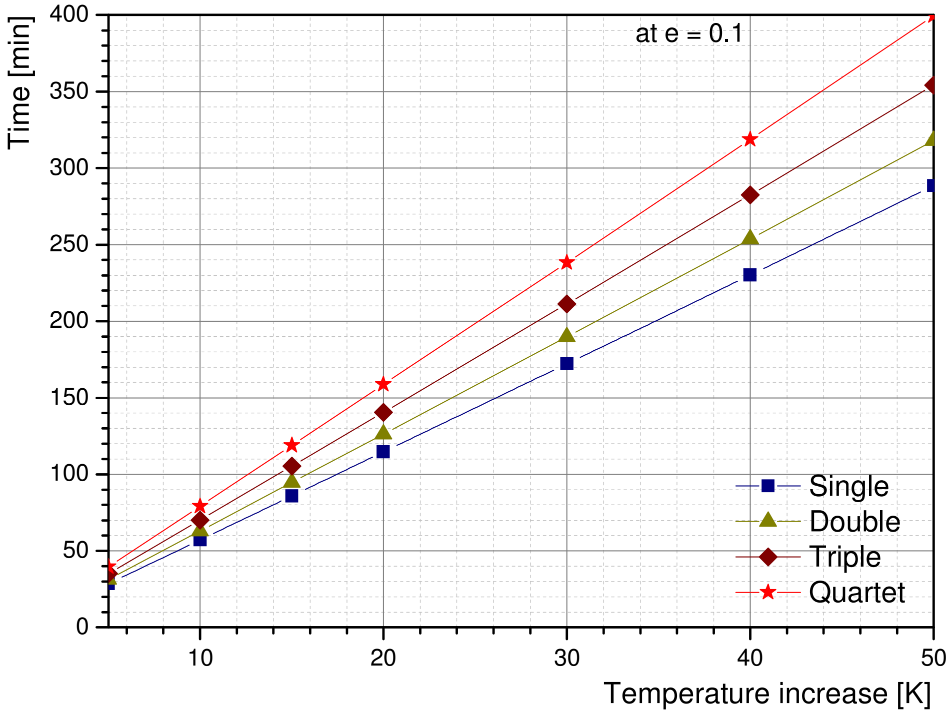

Fig. 9. Temperature development in dependence on detector configuration and ε=0.1.

As it has been seen even by single detector and emissivity of 0.2 there is approximately 30 min prior the detector is to be warmed by 10 K.

By an emissivity decrease from 0.2 to 0.1 the time needed for a temperature increase of 10 K rises to 58 min for the single configuration and from 35 min to 70 min for the triple detector.

As a comparison, the warming up of a single HPGe detector with 15% efficiency (commercially available PopTop), which corresponds of 344 g Ge is presented on Fig.10. The warm up time is evaluated based on typical crystal housing sizes and also is presented on Fig.8-9.

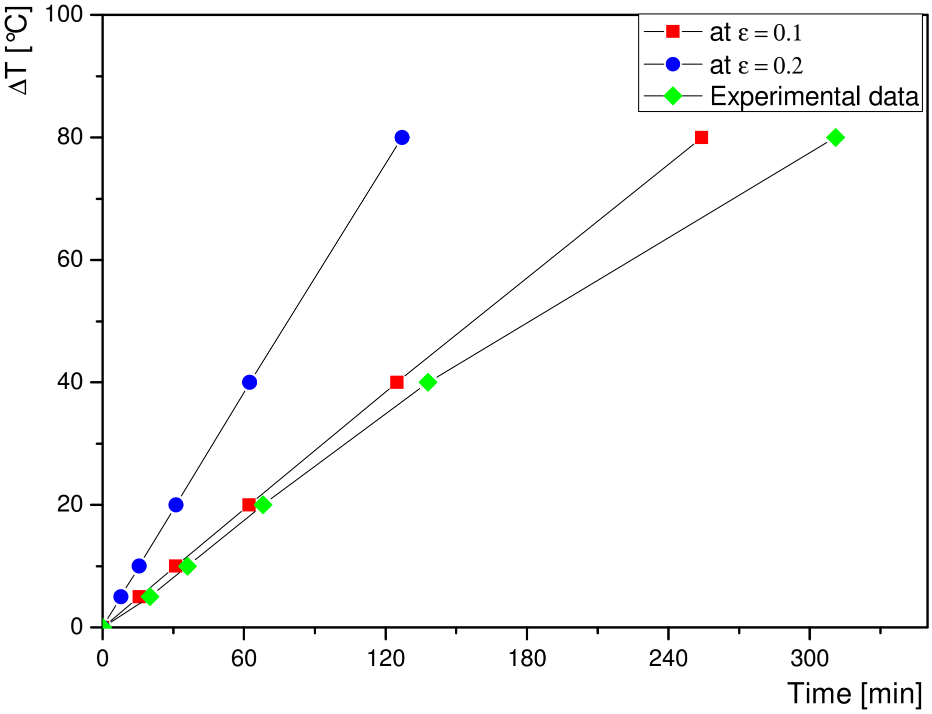

Fig.10. Warming up of a single HPGe detector with 15 % efficiency.

The warming up phases of a single detector has been numerically calculated (assuming emissivity of 0.2) and the results are presented on Fig.11. Based on 77 K cold part temperature and 300 K warm aluminum detector cup temperature, the heat loads has been evaluated and found to be 450 W/m².

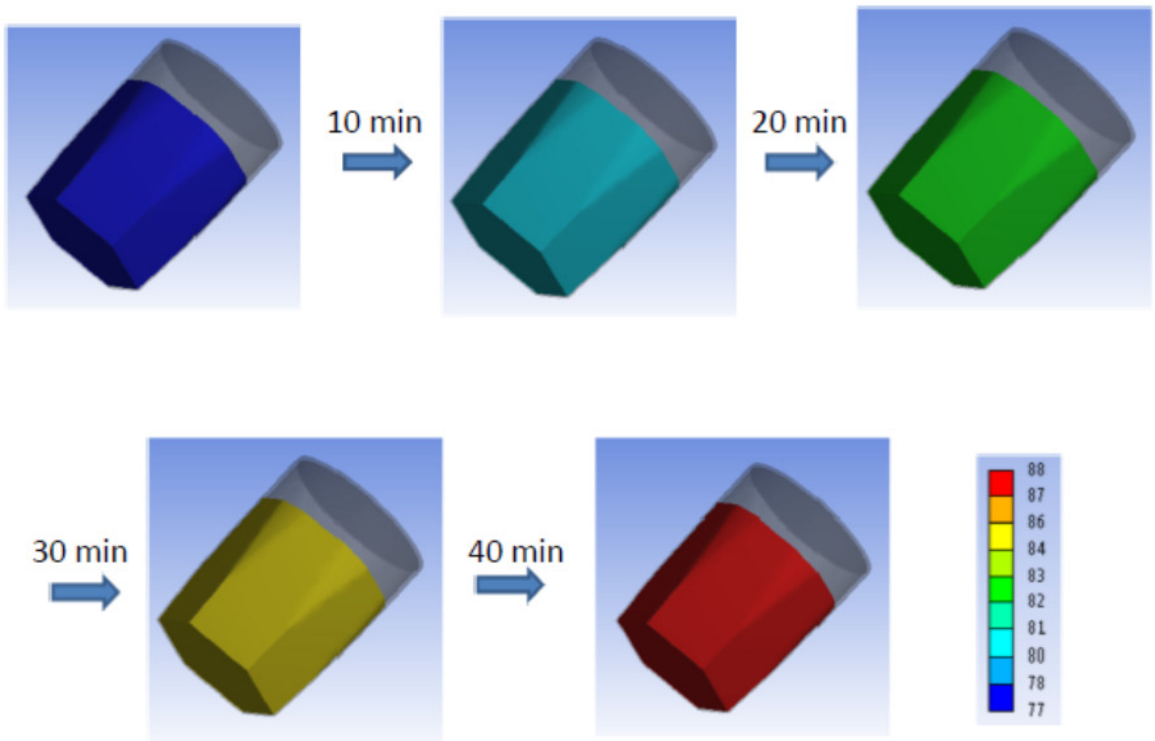

Fig. 11. Temperature increase of the HPGe detector in stand-alone regime.

The detector cooling has been estimated when the cooling engine with cooling power Q has been switched on. Assuming constant cooling power Q of the engine, the cooling time $t_{cooling}$ is determined by

$$t_{cooling} = t_{ref} \cdot \left\{ -\frac{1}{4\sqrt{2}a} \cdot \left[ln\frac{\theta^2+\sqrt{2}a\theta+a^2}{\theta^2-\sqrt{2}a\theta+a^2} + 4 \cdot arctan\frac{\sqrt{2}a\theta}{\sqrt{a^4+\theta^4}+a^2-\theta^2} \right] + \frac{1}{4\sqrt{2}a} \cdot \left[ln\frac{1+\sqrt{2}a+a^2}{1-\sqrt{2}a+a^2} + 4 \cdot arctan\frac{\sqrt{2}a}{\sqrt{a^4+1}+a^2-1} \right] \right\}$$

.

Here $= \frac{T}{T_\infty} = \frac{T_0+\Delta T}{T_\infty}$, $a^4 = 1 - \frac{Q}{\varepsilon\sigma T_\infty^4 A}$ and again $\theta_0 = \frac{T_0}{T_\infty}$, $\tau = \frac{t}{t_{ref}}$, , $t_{ref} = \frac{\rho c}{\varepsilon\sigma T_\infty^3} \cdot \frac{V}{A}$.

In Fig. 12-15 the detector cooling processes is presented in dependence of surface emissivity. The cooling power of 3 W has been supposed.

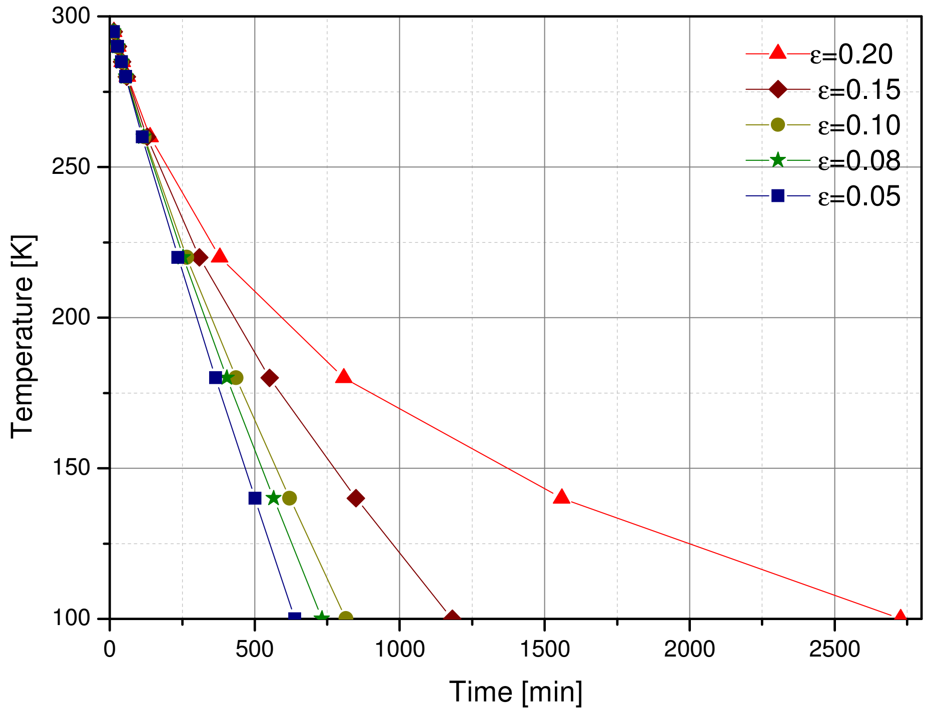

Fig. 12. Single detector cooling in dependence of emissivity.

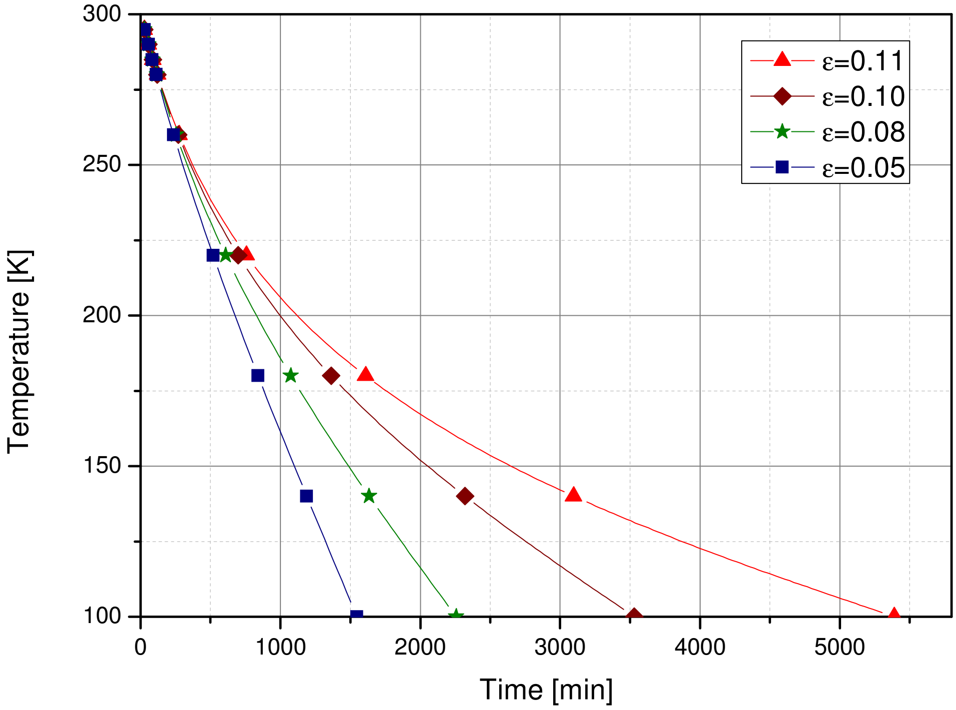

Fig. 13. Double detector cooling in dependence of emissivity.

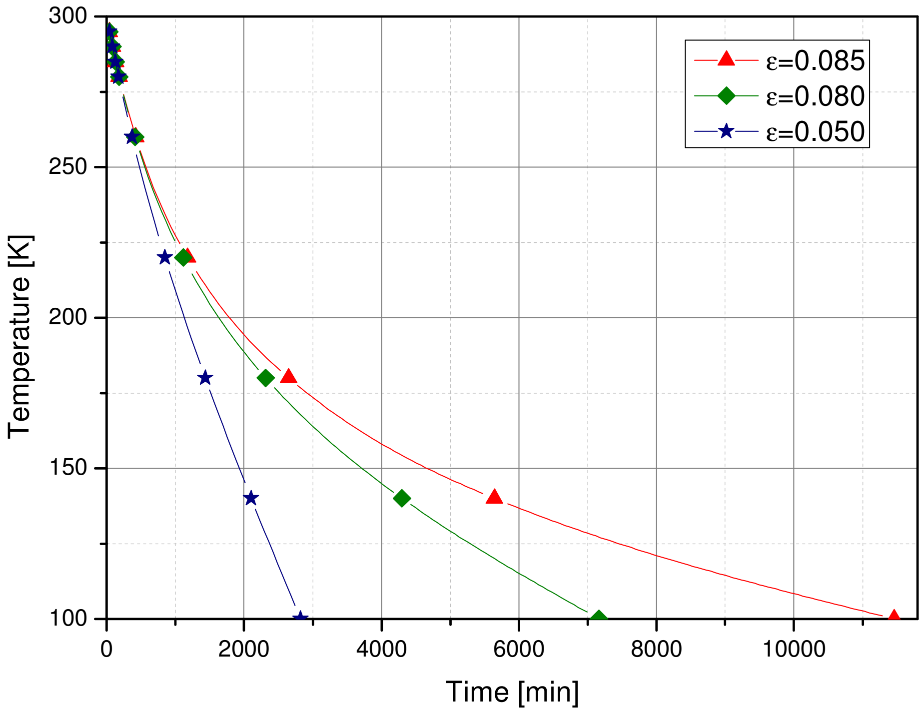

Fig. 14. Triple detector cooling in dependence of emissivity.

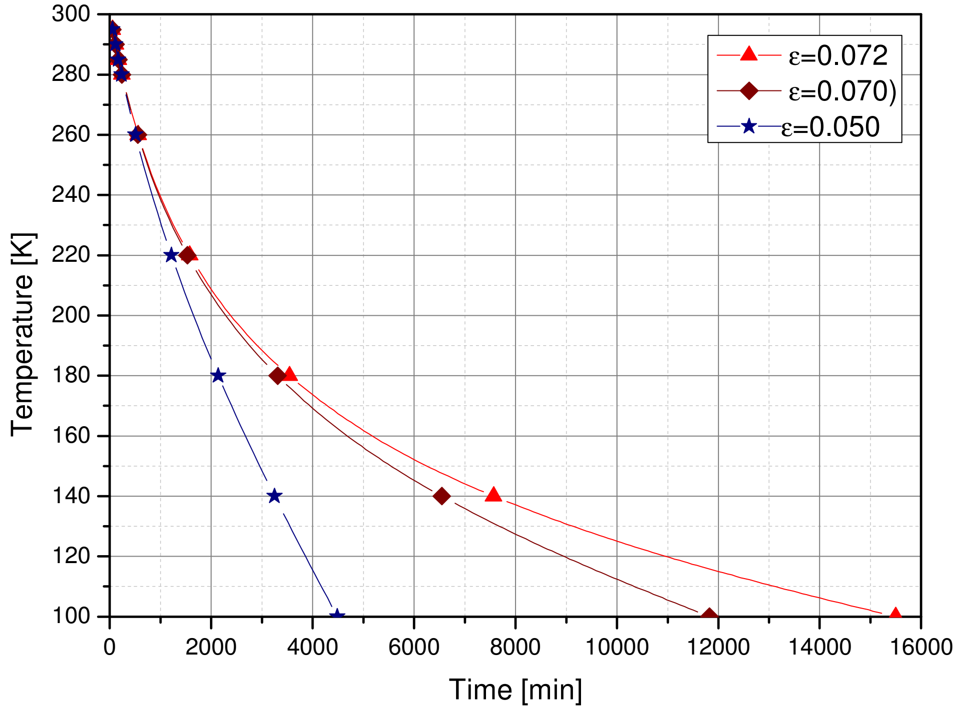

Fig. 15. Quartet detector cooling in dependence of emissivity.

On Fig. 16 is given the cooling of the electrically cooled single EB capsule.

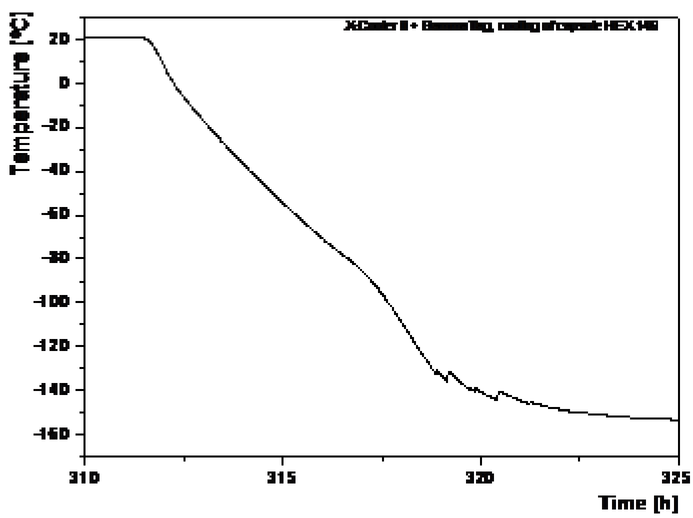

Fig.16. Cooling time of the electrically cooled single EB capsule.

The thermal expansion coefficient reduces with decreasing temperature; minor temperature variations take place below 77 K. Furthermore, these variations are similar for almost all material. The data available, critically investigated by the NIST, is graphically presented in Fig. 17. The study of the thermal expansion has relevance to the thermal stresses which appears at some critical holding structures.

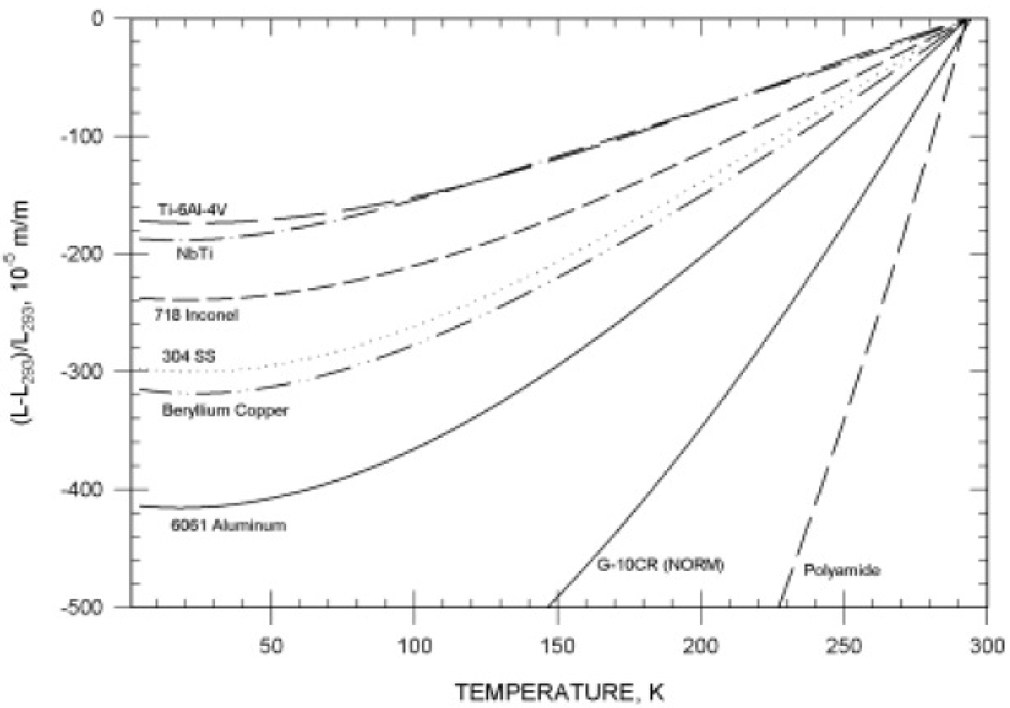

Fig. 17. Linear thermal expansion of various materials [3].

2.3. Thermal radiation at cryogenic temperature

Thermal radiation is the main effect which determines the total heat transfer of the detector head assembly. The cold inner assembly (detector capsules, cold finger and the cold frame) is at near LN2 temperature and the outer warm assembly – the cryostat walls, at room one. The heat transfer depends on the emissivity of the component materials and its value is governed by the matter of these materials, the surface finish, radiation wavelength and the angle of incidence. For materials of technical interest, measured average values are found in the literature [8, 9, 10], a subset of which is given after Woodcraft [11] in Table 4. As a general rule, emissivity decreases at low temperature, for good electrical conductors and for polished surfaces.

Material	Emissivity
Polished cooper	0.02-0.04
Lightly oxidized cooper	0.1
Highly oxidized cooper	0.6
Polished aluminum (pure and alloys)	0.01-0.06
Highly oxidized aluminum	0.2
Gold	0.015-0.03

Table 4. Emissivity coefficients.

From this table can be seen that a polished cooper or aluminum surface would nicely fit to the low emissivity requirement. However, such a surface is difficult to protect against oxidation, particularly if handled, and in practice gold plating would be the best solution.

It is worth to point out that the peak wavelength of thermal radiation change with temperature, and thus measurements of emissivity at room temperature must be cautiously applied to cryogenic systems.

Another obstacle arises from the fact that optical studies are typically performed under stringent conditions of surface treatment and the prediction based on them do not include the effects connected with real surfaces as they are used in cryogenics.

A systematical study of low temperature properties of materials used in cryogenics is represented in [12] and some data are graphically here in order to give an idea of how the emissivity depends on temperature at cryogenic temperature.

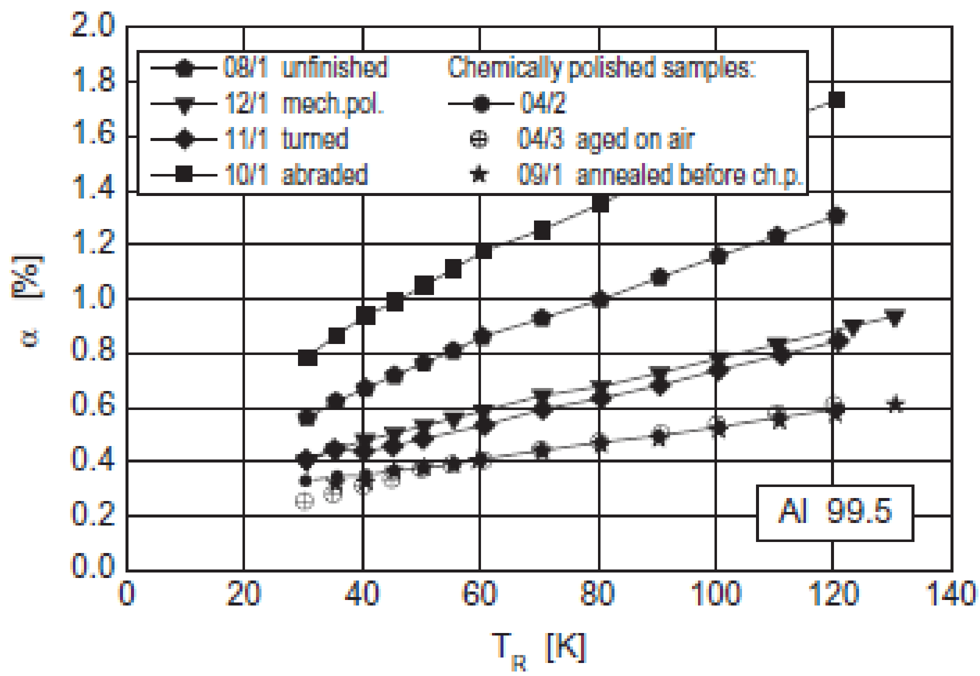

Fig. 18. Total hemispherical emissivity of Al 99.5 sheet with a various surface treatment [12].

The data on emissivity at low temperatures at various temperatures of radiated and irradiated surfaces is summarized in [13] and [14] and the data are reproduced in Table 5.

Material	Radiation from 290 K	Radiation from 77 K

	Surface at 77 K	Surface at 4.2 K
Stainless steel, as found	0.34	0.12
Stainless steel,mech. polished	0.12	0.07
Stainless steel, electro polished	0.10	0.07
Stainless steel + Al foil	0.05	0.01
Aluminum, as found	0.12	0.07
Aluminum, mech. Polished	0.10	0.06
Aluminum, electro polished	0.08	0.04
Cooper, as found	0.12	0.06
Cooper, mech. Polished	0.06	0.02

Table 5. Emissivity of technical materials at low temperatures.

2.4. Insulation materials under vacuum

Early evaluation of the heat transfer in a single capsule assembly [5] has suggested that the domination of the radiative transfer is enormously strong. The triple assembly and even the doublet have much larger surface subjected to radiative transfer and therefore, the impact of this transfer should be even stronger. Applying radiative shield is not realistic due to the complicated shape of the assembly. A way to reduce the heat transfer by infrared radiation would be the use of superinsulation (multilayer insulation, MLI). In this case the radiative transfer would be “replaced” by conductive heat transfer and facilitated by MLI, may have very low value.

Superinsulation is identified with diathermancy significantly lower than those of air. That condition has been achieved either by evacuated loose granulated material or by evacuated reflecting metal foil (s. Fig. 19 after [15]).

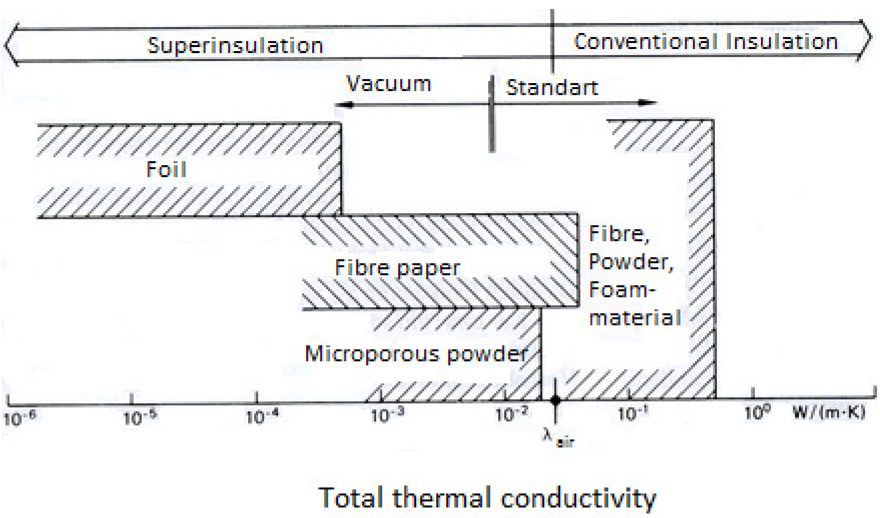

Fig. 19. Summary of the achievable total thermal conductivity from superinsulation under low temperature [15].

Generally the development of the modern insulation technic under cryogenic temperature can be traced through three patents [16, 17, 18] filled by Dana (1939), Cornell (1947) and Matsch (1956). The first patent gives details for a double-walled tank with the annular space evacuated and filled with finely divided solid material while the second one outlines details for radiation shielding of containers by use of multiple polished tank walls within the outer tank. The

A schematic depiction of the foil insulation assembly is shown after [15] in Fig. 20.

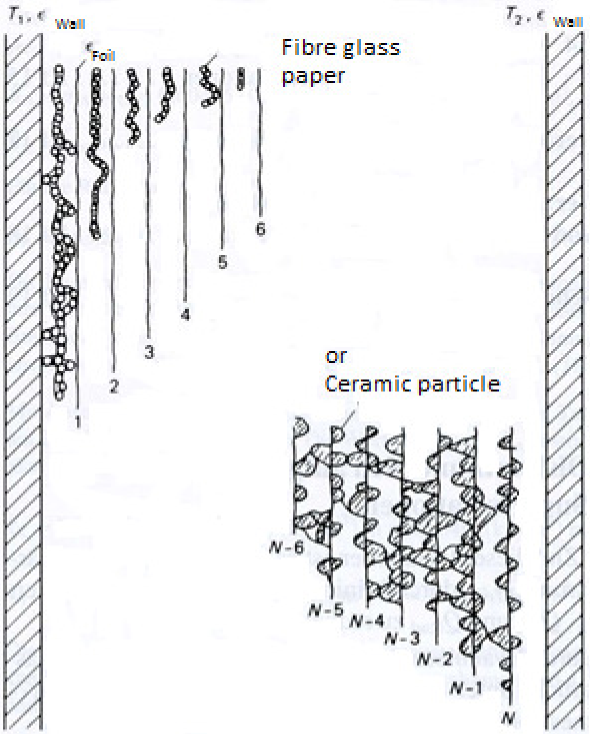

Fig. 20. Foil insulation assembly [15].

Systems using evacuated powders or fibers require a good vacuum level to be fully effective. Nevertheless, the evacuated powder systems have the tendency to settle and compact due to vibration or thermal cycling, which in turn leads to degradation of thermal performance and possible structural damage.

Some representative experimental total thermal conductivity values for different materials and the reference case boundary temperature of approximately 80 and 300 K are referred in [18, 19] and hire given in Table 6.

Material System	K-Value (mW/m-K)		Vacuum (torr)		Reference
Cellular glass foam, 128 kg/m^3 (190 K)	33		760		Vendor data
Polyurethane foam, 32 kg/m^3 (190 K)	21		760		13
Fiberglass, 16 kg/m^3	2	14	10^{-4}	1.0	Vendor data
Perlite powder, 128 kg/m^3 (190 K)	1.5	16	10^{-4}	1.0	1
Aerogel/fiber composite, 125 kg/m^3	0.55	3.3	10^{-4}	1.0	8
Microspheres, uncoated, 73 kg/m^3	0.59		10^{-6}		5
Vacuum, polished surfaces	0.5 to 5.0		$<10^{-5}$		9
MLI, foil and paper, 60 layers @ 2.8/mm	0.08		$6x10^{-5}$		3
MLI, foil and paper, 50 layers	0.06	18	$4x10^{-5}$	1.0	10
MLI-ultimate	~0.02		$<10^{-5}$		2

Table 6. Experimental thermal conductivity values for different materials.

In order to give an idea of how the heat transferred is influenced by the interstitial gas pressure the Fig. 21 after Hoffmann [20] is given below.

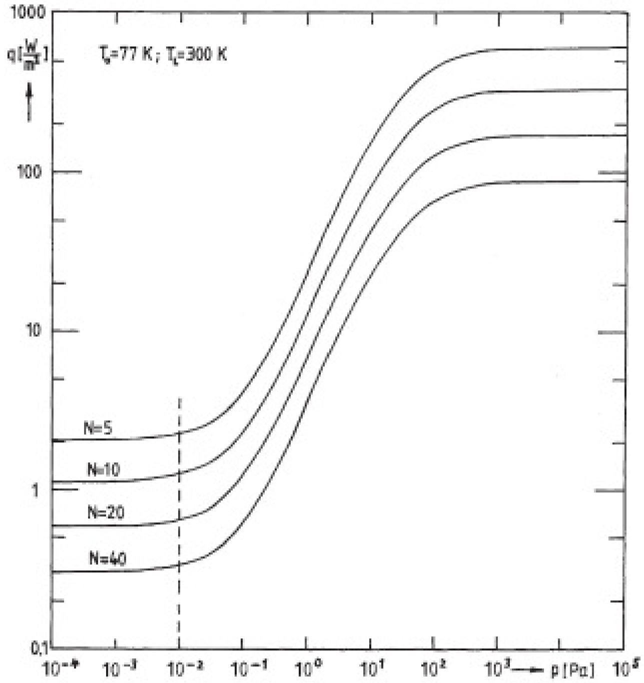

Fig. 21. The heat flux density as a function of the interstitial gas pressure with the number of layers N as parameter at standard temperature conditions.

Systematically measurement to determine the insulation efficiency of a multilayer blanket manufactured by Jehier (Chemille, France) has been performed at NASA Kennedy Space Center by Fesmire et al. [22]. The total thickness of the 30 layers blanket tested was 7 mm (density of 4.3 layers/mm).

The results presented by Fesmire et al. [22] are shown hire in Fig. 22 and Fig. 23.

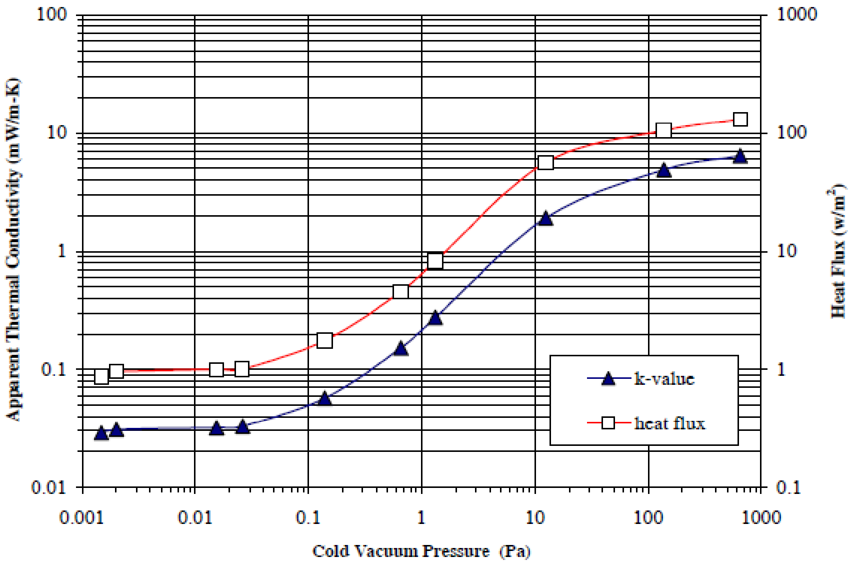

Fig. 22. Variations of apparent thermal conductivity (k-value) and heat flux with cold vacuum pressure (CVP).

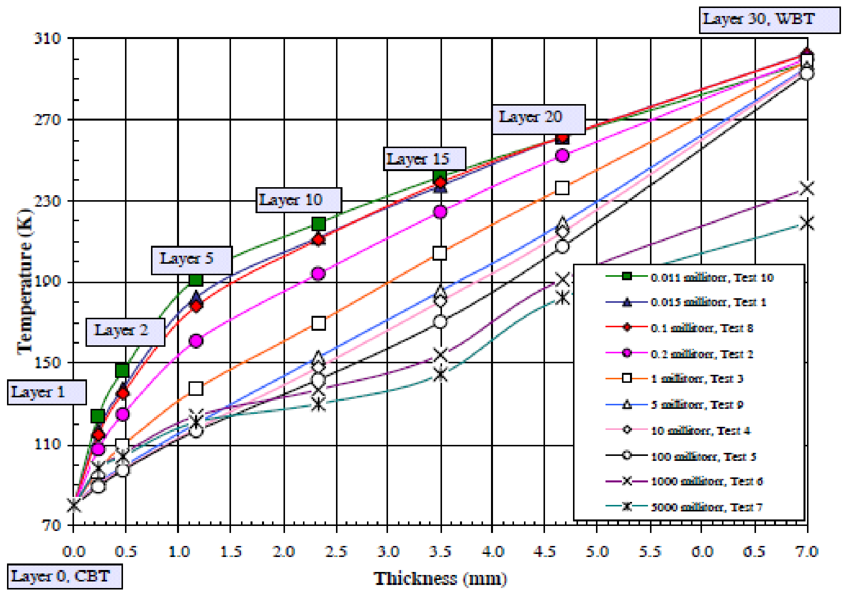

Fig. 23. Variation of layer temperatures with blanket thickness for different cold vacuum pressures (1 millitorr = 0.1333 Pa).

Thereon, it seems to be feasible a prefabricated blanket multilayer to be applied as capsules assembly insulation in order to minimize the detector head warming.

For the flexible cold finger a suitable solution might be searched among the granulated materials for instance micro glass spheres.

3. Analysis of the heat transfer within the HPGe Assembly under the primary accent on material, shape and site optimisation of the fixing labyrinth.

The fixing labyrinth acts as mechanical integration fixture of the cold and warm structures of the cryostat (s. Fig. 2). Simultaneously it acts as a thermal bridge between the warm and the cold part of the assembly.

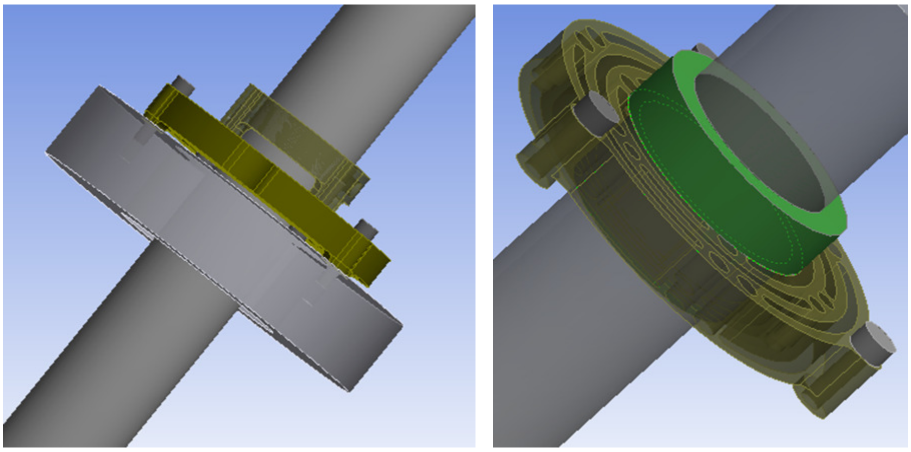

Fig. 24. Cold finger fixing assembly: left new design, right old design.

Various fixing constructions have been implemented. The widely spread one is an insulating labyrinth with metal sleeve which fixes the labyrinth itself to the cold finger. To such an extent the mechanical strength of the construction becomes also important. The detail drawing is shown in Fig. 24: left new design, right old one.

Now in order to minimize the heat transmitted, the contact between the plastic labyrinth and the metal sleeve should not be any longer the whole overall upper surface of the metal peace but only thin bridges.

As the material characteristics of the both components determined the heat resistance of the fixing assembly first the influence of the sleeve material on the total heat transfer has been examined. In Fig. 25 the temperature distribution along the surface of the Vespel fixing labyrinth and the stainless steel sleeve is shown. The temperature of the warm part is considered to be 295 K and of the cold finger 100 K.

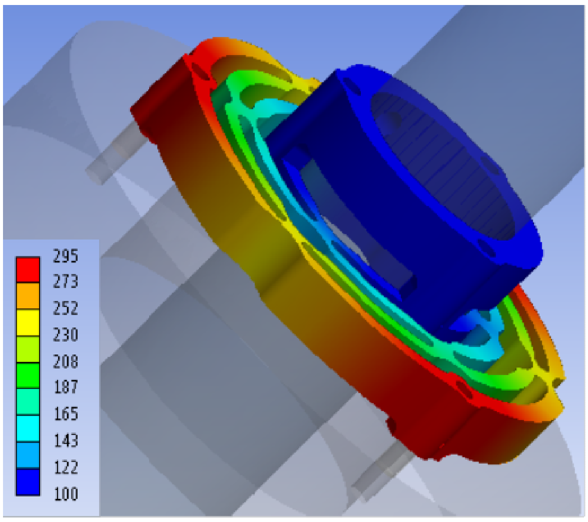

Fig. 25. Temperature distribution along the surface of the Vespel fixing labirinth and the stainless steel sleeve.

By the new design the sleeve material (stainless steel or aluminium) is found to influence negligible, less than 1 % the transmitted heat and thus the material choice is to be based on the manufacturing cost and mechanical strength.
Then the heat losses as a function of the fixing labyrinth material as well as cold finger temperature are studied and the data obtained are summarized in Table 7. All the material considered satisfied the specification as the heat losses are below 0.1 W.

Material	**Cold Finger Temperature [K]**	**Heat Losses [x 10^{-2} W]**
Kapton	70	4.42
	100	3.96
	115	3.70
Teflon	70	6,89
	100	6,06
	115	5,62
Nylon	70	8,80
	100	7,76
	115	7,19
Vespel	70	7,66
	100	6,64
	115	6,13

Table 7. Heat losses in dependence on the fixing part material and the cold finger temperature.

References:

1. I. Kojouharov, T. Engert, J.Gerl, J. Kojouharova, M.Steinen, A.Sanchez-Lorente, J.Pochodzalla, Composite Germanium Detector with Electromechanical Cooling, 3rd ASPERA Technology Forum Industry meet Academia, 13-14 March 2012 Lichtenberg-Haus, Darmstadt.

2. I. Kojouharov, Electrically Cooled Ge-Detectors development: Status Report, PANDA, GSI, 6. September 2010.

3. E.D. Marquardt, J.P. Le, and Ray Radebaugh, Cryogenic Material Properties Database, National Institute of Standards and Technology, Boulder, CO 80303.

4. A. L. Woodcraft, and A. Gray, A low temperature thermal conductivity database, CP1185, Low Temperature Detectors LTD 13, Proceedings of the 13th International Workshop (2009), ed. by B. Cabrera, A. Miller, and B. Young American Institute of Physics, 681-684.

5. I. Kojouharov, H.-J. Wollersheim, J. Kojouharova, J. Gerl, M. Wolf, T. Engert, Encapsulated Germanium Detector with electromechanical cooling, GSI Scientific Report 2008, Instruments-Methods-19.

6. J. Kojouharova, M. Wolf, H.-J. Wollersheim, Simulierte Kühlung, Physik-Journal, Sonderheft „Best of“, September 2008, 46-47.

7. J. Kojouharova, S. Lago, H.-J. Wollersheim, I. Kojouharov, J. Gerl, Study of operational characteristics of pixelated Germanium Detector, 11th National Congress on Theoretical and Applied Mechanics, 2-5 Sept. 2009, Borovets, Bulgaria, P1-P10.

8. W. Obert et al., Emissivity measurements of metallic surfaces used in cryogenic applications, Adv. Cryo. Eng. 27, 1982, 293.

9. G. K.White and P. J. Meeson. Experimental techniques in low-temperature physics. Oxford: Clarendon Press, 4th edition, 2002.

10. Ed. B. Hands. Cryogenic Engineering. Academic Press, London, 1984.

11. A. Woodcraft, An introduction to cryogenics, http://uk.lowtemp.org/1-Woodcraft.pdf

12. V. Musilova, P. Hanzelka, T. Kralik, A. Srnka, Low temperature properties of materials used in cryogenics, *Cryogenics* **45,** 2005, 529-536.

13. Ph. Lebrun, Introduction to Cryogenics, CAS & ALBA School on Vacuum in Accelerators, Platya d’Aro, Spain, 16-24 May 2006.

14. Ph. Lebrun, Introduction to Cryogenics, Departmental Report, Commission A1 “Cryophysics and Cryoengineering” of the IIR Accelerator Technology Department, CERN, Geneva, Switzerland, CERN/AT 2007-1, 1-25.

15. VDI-Wärmeatlas: Berechnungsblätter für den Wärmeübergang, Hrsg. Verein Deutsche Ingenieure; VDI-Gesellschaft Verfahrenstechnik und Chemieingenieurwesen, Springer, 2002.

16. L. Dana, 1939, Insulated container for liquefied gases and the like, US Patent No. 2,396,459.

17. W. Cornell, 1947, Radiation shield supports in vacuum insulated containers, US Patent No. 2,643,022.

18. L. Matsch, 1956, Thermal insulation, US Patent No. 3,007,596.

19. S. D. Augustynowicz, J. E. Fesmire, and J. P. Wikstrom, Cryogenic insulation systems, 20ta International Congress of Refrigeration, IIR/IIF, Sydney, 1999.

20. J. E. Fesmire, S. D. Augustynowicz, Cryogenic Thermal Insulation Systems, 16th Thermal and Fluids Analysis Workshop, Orlando, Florida, August 9, 2005.

21. A. Hofmann, The thermal conductivity of cryogenic insulation materials and ist temperature dependence, Cryogenics 46 (2006), 815-824.

22. J. E. Fesmire, S. D. Augustynowicz, C. Darve, Performance characterization of perforated multilayer insulation blankets